THE JOURNAL OF PHYSICAL CHEMISTRY Letters

Letter

pubs.acs.org/JPCL

Nanotube-Enabled Vesicle−Vesicle Communication: A Computational Model

Liuyang Zhang and Xianqiao Wang*

College of Engineering and NanoSEC, University of Georgia, Athens, Georgia 30602, United States

ABSTRACT: Cell-to-cell communications via the tunneling nanotubes or gap junction channels are vital for the development and maintenance of multicellular organisms. Instead of these intrinsic communication pathways, how to design artificial communication channels between cells remains a challenging but interesting problem. Here, we perform dissipative particle dynamics (DPD) simulations to analyze the interaction between rotational nanotubes (RNTs) and vesicles so as to provide a novel design mechanism for cell-to-cell communication. Simulation results have demonstrated that the RNTs are capable of generating local disturbance and promote vesicle translocation toward the RNTs. Through ligand pattern designing on the RNTs, we can find a suitable nanotube candidate with a specific ligand coating pattern for forming the RNT−vesicle network. The results also show that a RNT can act as a bridged channel between vesicles, which facilitates substance transfer. Our findings provide useful guidelines for the molecular design of patterned RNTs for creating a synthetic channel between cells.

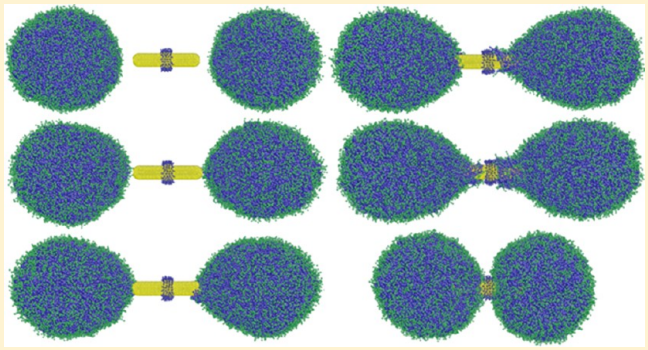

Cell-to-cell communication and exchange of materials are vital for the development and maintenance of multicellular organisms.[1−4] To achieve efficient communication, organisms have evolved multiple strategies, which include direct physical contact or long-range interactions mediated by endocrine mechanisms.[5] Typically, cells communicate with one another using diffusible signal molecules. An efficient pathway for cell-to-cell transmission of the signal molecules between individual cells plays an important role in the development of cellular activities. Besides these intrinsic communication pathways, how to design artificial communication channels between cells for the development and maintenance of multicellular activity remains a challenging but open question.

Experiments have shown that cells are capable of communicating between adjacent cells via direct contact through gap junctions.[5,6] Gap junctions are channels that allow for the transport of ions, nutrients, and other substances and enable cells to communicate. The basic building block of each gap junction is the connexin subunit. Six of these subunits in each of the membranes of two neighboring cells come together, and then, the group of six connexins in one cell interacts with a comparable hexamer in the other cell, resulting in the formation of a channel.[5] Gap junction channels can vary the permeability and selectivity of a membrane in response to various internal and external factors including cytosolic Ca^{2+}, membrane potential, connexin phosphorylation, electromagnetic fields, temperature, and pH in the environment.[7] Between distant cells, a general and dynamic membrane nanotube (MNT) (1/500th the thickness of a human hair) found in plant and animal cells was discovered to be involved in cell-to-cell communication.[8−10] For example, the MNT, formed when T cells make contact and subsequently part, provides a new route for HIV-1 transmission, which has been estimated to be as much as 100−1000 times more efficient than a tube-free process.[11] The MNT also allows human natural killer (NK) cells to interact functionally with target cells over long distance.[12] However, different from the inherent biocomponent of a intercellular junction or MNT from cells, the synthetic cell-to-cell communication medium remains unexplored.

Exotic nanoparticles (NPs) such as synthetic DNA and carbon nanotubes (CNTs) have been reported as developing synthetic analogues of biological membrane channels, and they possess high efficiency and remarkable selectivity for transporting ions and molecules into cell interiors.[13−17] Self-assembled DNA origami was used to create a stem that penetrated and spanned a lipid membrane as well as a barrel-shaped cap that adhered to the membrane.[16] Short CNTs can spontaneously insert into lipid bilayers and live cell membranes to form channels that exhibit a unitary conductance of 70−100 picosiemens under physiological conditions.[13] However, preparation of a large number of samples is typically required, and each sample has local discrepancy with others, which makes the experiments difficult to attribute the particular phenomenon to a single parameter. With the aid of computational simulations, a quantitative analysis of interactions between NPs and lipid layers can be obtained. For example, by dissipative particle dynamics (DPD) simulations, end-functionalized

Received: April 10, 2015
Accepted: June 16, 2015

DOI: 10.1021/acs.jpclett.5b00755
J. Phys. Chem. Lett. 2015, 6, 2530−2537

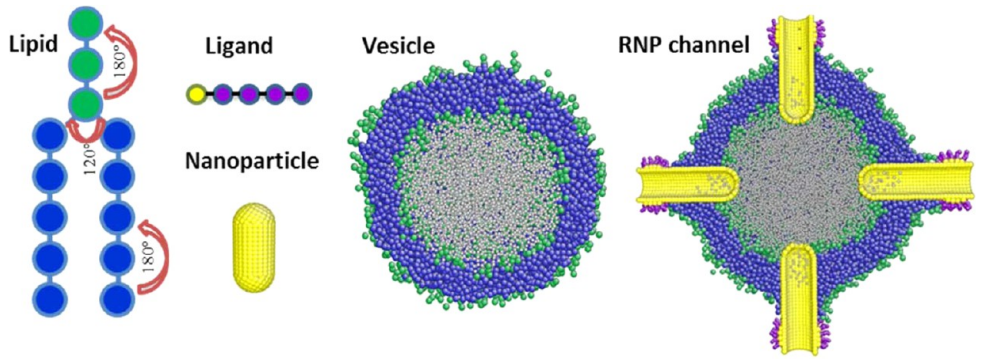

Figure 1. Schematic representation of the DPD model. In the figure, unless otherwise stated, the hydrophobic beads are shown in blue while the hydrophilic beads are shown in green. The length of the ligand is fixed as 5 (1 hydrophobic bead in yellow and 4 hydrophilic beads in purple). The RNT is shown in yellow. For clarity, the water outside of the vesicle is not shown in all figures.

nanotubes were stabilized in the membrane to form the transmembrane channel.[18] A number of simulations suggest that the membrane translocation of anisotropic NPs is often accompanied by active and passive rotation of the NPs. The penetrating effect of an active NP rotation is ascribed to enhanced membrane monolayer protrusion as well as the exertion of a shearing force, which can rupture the membrane.[19] Ligand-coated NPs with anisotropic patterns and a graphene sheet are passively rotated to a preferred orientation while penetrating through the membrane.[20,21] Experimental work has demonstrated that active rotation of NPs can be controlled by an underlying dynamic magnetic field.[22,23] For example, the rotational movement of superparamagnetic iron oxide NPs induced by a dynamic magnetic field causes membrane permeabilization and leads to apoptosis.[24] By virtue of the paramagnetic nature of multiwalled CNTs (MWCNTs), they rotate when exposed to a weak rotating magnetic field and therefore damage the viability of tumor cells.[25] NPs are enclosed inside of intracellular endosome vesicles, which can be deformed to probe the intracellular membrane, or turned into intracellular heaters when subjected to a magnetic field.[26,27] However, there is little work unraveling the fundamental mechanism of how a cell responds to an active rotational nanotube (RNT), which hinders our understanding toward a better drug/gene delivery system.

In this Letter, by using DPD simulation, we will mimic cell-to-cell communication by proposing a synthetic RNT channel bridging the vesicles. We first propose a simple magnetic field geometry to create a RNT channel on a single vesicle. Second, we demonstrate that the RNT channel could bridge the vesicle to form the RNT−vesicle network, where the RNT channel allows vesicular communication via a diffusive process. Analysis of the mechanism underlying the interaction between RNTs and vesicles will provide insight into the molecular dynamics of cellular features. Our simulation results can establish the RNT as a promising prototype of synthetic membrane channels to bridge single cells into a bionetwork with inherent robustness geared toward biological challenges and exceptional biocompatibility for cell-to-cell communication.

Computational Model and Methodology. Simulations in this Letter are based on DPD, a very successful mesoscopic coarse-grained simulation method for soft matter and biomembrane systems.[28,29] In DPD simulations, a small group of atoms is treated as a single bead located at the center of mass of the group. Beads i and j interact with each other via a pairwise force consisting of a conservative force F_{ij}^{C} representing the excluded volume effect, a dissipative force F_{ij}^{D} representing viscous drag between moving beads, and a random force F_{ij}^{R} representing stochastic impulse. Both F_{ij}^{D} and F_{ij}^{R} act together as a thermostat for the beads. Similar to molecular dynamics simulation, time evolution is also governed by Newton's equation of motion. The total force on bead i can be expressed as

$$F_i = \sum_{i \neq j} (F_{ij}^{C} + F_{ij}^{D} + F_{ij}^{R})$$
$$= \sum_{i \neq j} (a_{ij}\omega(r_{ij})\hat{r}_{ij} - \gamma\omega^2(r_{ij})(\hat{r}_{ij}\cdot v_{ij})\hat{r}_{ij} + \sigma\omega(r_{ij})\zeta_{ij}\Delta t^{-1/2}\hat{r}_{ij})$$

where a_{ij} is the maximum repulsive force, r_{ij} the distance, $\hat{r}_{ij}$ the unit vector, and v_{ij} the relative velocity between beads i and j; ζ_{ij} denotes a random number with zero mean and unit variance, and

$$\omega(r_{ij}) = \begin{cases} 1 - \dfrac{r_{ij}}{r_c} & r_{ij} < r_c \\ 0 & r_{ij} > r_c \end{cases}$$

is a normalized distribution function, r_c being the cutoff radius; γ and σ are parameters related to each other as $\sigma^2 = 2\gamma k_B T$, $k_B T$ being the unit energy. The standard values $\sigma = 3.0$ and $\gamma = 4.5$ are used in our study.[20] The mass, length, and time scales are all normalized in the DPD simulations, with the unit length taken to be the cutoff radius r_c, the unit mass to be that of the solvent beads, and the unit energy to be $k_B T$. All other quantities are expressed in terms of these basic units. The reduced DPD units can be converted to SI units by examining the membrane thickness and the lipid diffusion coefficient. The simulated value of the bilayer thickness is $5r_c$ and the effective time scale of simulation can be determined from the simulated lateral diffusion constants of the lipid bilayer.[30] The DPC bilayer thickness is about 4 nm with a diffusion coefficient of around 5 $\mu m^2\ s^{-1}$;[31] by comparison with typical experimental values, it can be shown that one DPD length unit corresponds to approximately 0.8 nm in physical units and the time unit to τ = 24.32 ps. The time step is taken as $\Delta t = 0.01\tau$. All simulations are performed using LAMMPS.[32]

The dimension of the simulation box here is $50r_c \times 50r_c \times 75r_c$. The simulation system consists of the vesicle consisting of 2250 lipid molecules and a rigid cylindrical RNT (composed of 1515 hydrophobic beads) coated with a selected pattern of ligand and solvent particles. The lipid molecule is represented by the coarse-grained model proposed by Groot and Rabone,[28]

DOI: 10.1021/acs.jpclett.5b00755
J. Phys. Chem. Lett. 2015, 6, 2530−2537

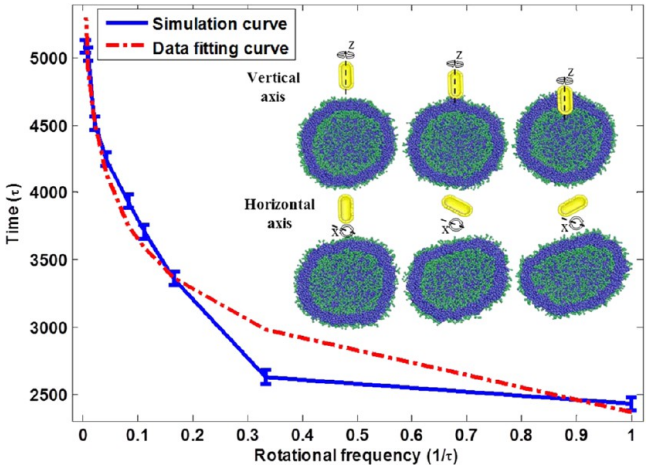

Figure 2. Contact time of the RNT and vesicle versus the rotational frequencies of the RNT. The snapshots depicts vesicle responses to the RNT with different rotational axes, a vertical axis and a horizontal axis.

as shown in Figure 1. The ligand consists of one hydrophilic bead and four hydrophobic beads. The solvent beads are not shown in figures for clarity. The particle density of the whole system is approximately 3.[33] The hydrophilic and hydrophobic beads are in green and blue, respectively. The repulsive interaction parameters between beads of the same type within the RNT, ligand, and membrane are taken as $a_{ij} = 25$, and those for two beads of different types are set as $a_{ij} = 100$. Within a lipid molecule and ligand, an elastic harmonic force

$$F_{ij}^{S} = k_S\left(1 - \frac{r_{ij}}{r_S}\right)\hat{r}_{ij}$$

is used to connect two consecutive beads, where k_S and r_S are the spring constant and equilibrium bond length, respectively. Here, we use $k_S = 100.0$ and $r_S = 0.7r_c$ for lipid molecules[34] and $k_S = 200.0$ and $r_S = 0.25$ for ligands.[20] The ligands are also anchored to the RNT surface by a spring force with $k_S = 200.0$ and $r_S = 0.25$ to prevent the rearrangement or detachment of coating ligands during the simulation. The bending resistance

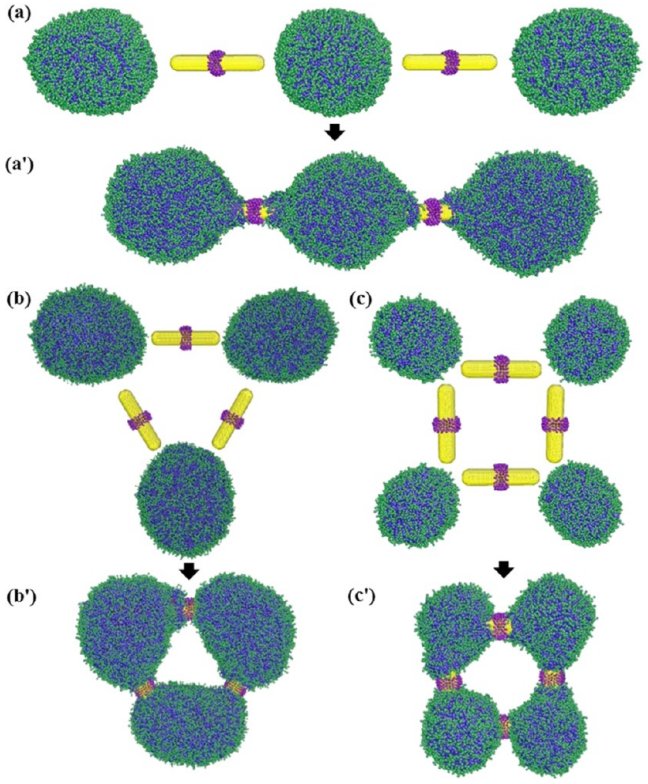

Figure 4. Multicomplex cellular network composed of RNTs and vesicles.

of the lipid and ligand chain is represented as an additional force due to a harmonic constraint on two consecutive bonds

$$F^{\theta} = -\nabla V_{\text{bend}} = -\nabla[k_\theta(\theta - \theta_0)^2]$$

where k_θ, θ, and θ_0 are the bending constant, inclination angle, and equilibrium angle, respectively. For three consecutive lipid tail beads or three consecutive lipid head beads in a lipid molecule, we take $k_1 = 6$ and $\theta_0 = 180°$; for the last head bead and the top tail beads, $k_2 = 3$ and $\theta_0 = 120°$; for the bottom two consecutive head beads and the first bead in each tail, $k_3 = 4.5$

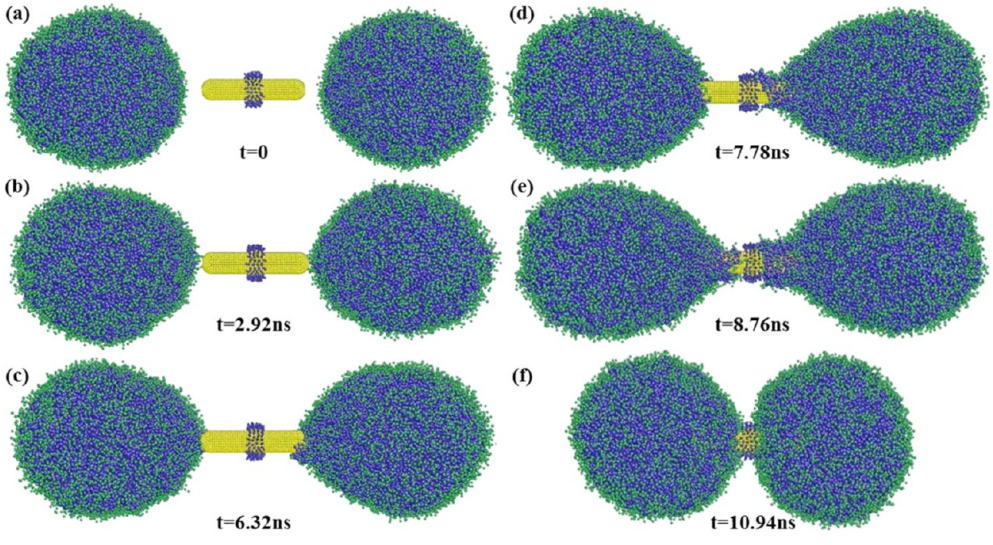

Figure 3. Dynamic evolution of a single RNT with two identical vesicles.

DOI: 10.1021/acs.jpclett.5b00755
J. Phys. Chem. Lett. 2015, 6, 2530−2537

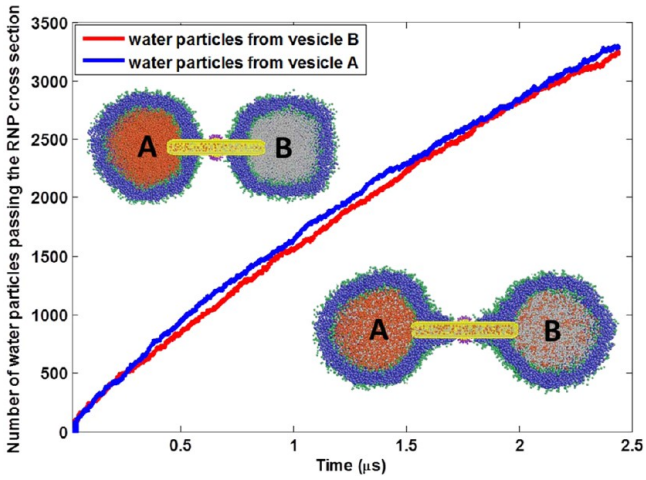

Figure 5. Evolution of water molecule transportation between two vesicles through the RNT channel. Water beads in vesicle A are shown in brown, while water beads from vesicle B are shown in white.

Table 1. Diffusion Rate of Water Particle for a Group of Two-Vesicle−One-RNT System

Pattern	Model	Radius	A to B (beads/ns)	B to A (beads/ns)
I	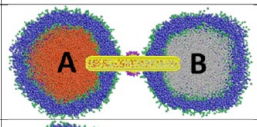	$12r_c$ $12r_c$	1.25	1.21
II	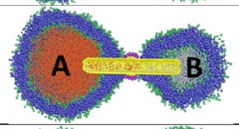	$12r_c$ $7r_c$	1.35	1.32
III	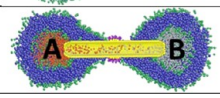	$7r_c$ $7r_c$	1.27	1.24

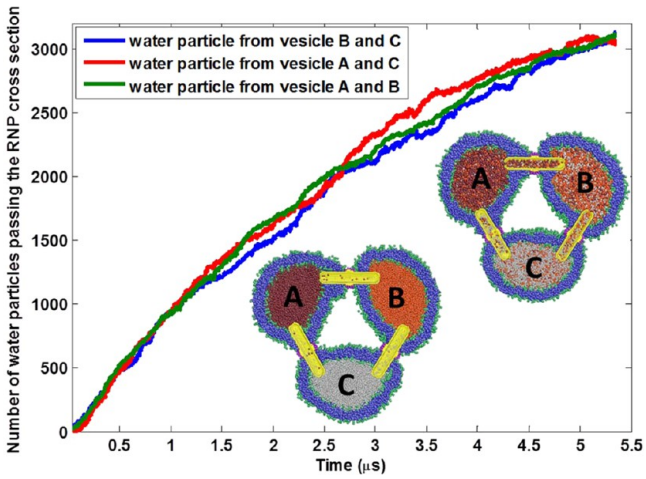

Figure 6. Evolution of water molecule transportation between three vesicles through the RNT channels. Water beads in vesicle A are shown in dark red, water beads in vesicle B are shown in brown, and water beads from vesicle C are shown in white.

and $\theta_0 = 120°$.[20] For three consecutive ligand beads, we take $k_\theta = 5$ and $\theta_0 = 180°$.

Rotational Frequencies. It has been shown that bacteria cells can move by rotating their long thin helical filaments to generate a forward motion.[35−37] Different from a filament-based rotor, the motor-like RNT can tremendously affect its local biological environment, thereby exerting undeniable influence on its penetration capability into biological tissues. For example, magnetic CNTs containing iron oxide NPs were also synthesized by the spray pyrolysis method and covalently attached the anti-pseudomonas antibody on the surface to develop a bioprobe for rapid identification of particular bacterium.[38] Magnetic iron oxide NPs were loaded onto the multiwalled CNTs surfaces by electrostatic self-assembling to afford magnetic nanotubes that were assembled onto red blood cells to form magnetic cells.[39] In our simulation, the resulting nanotube rotation, not attached to the vesicle but rather situated around the vesicle, causes synchronized translation of water particles to match the winding geometrical movement around the RNT.[40] Therefore, the water particle can induce a locomotive force on the vesicle along the rotational axis of the RNT to drive it toward the RNT rather than inducing random contributions with a zero net effect. As shown in Figure 2, initially the RNT (diameter = $4r_c$, length = $10r_c$) is placed $5r_c$ away from the vesicle surface and restrained to its center-of-mass during the rotation. We consider it as a default simulation model unless otherwise stated. As shown in Figure 2, along the long axis of the RNT, the vesicle is capable of approaching the RNT. In contrast, along the horizontal axis, the vesicle is pushed away by the RNT and has a noticeable morphological shape. The rotational axis is chosen to be the longitudinal axis of the nanotube for the reason that it could enhance the vesicle membrane protrusion as well as exert minimal shearing force to avoid the rupture of vesicle.[19] It has been demonstrated that the magnetic nanotube could be assembled and positioned in a controlled manner[41−43] and rotate with a controlled angle and speed by the magnetic field.[44,45] To investigate the effect of rotational frequencies on the process of nanotube penetration behavior, we assume that the sizes of the RNT and vesicle are fixed and an active rotation is applied to the RNT with a variety of different rotational frequencies, which generates the locomotive force necessary to drive the vesicle slowly toward the hydrophobic RNT. The translocation path of the vesicle is perpendicular to the vertical rotation surface of the RNT. Figure 2 indicates the translocation time needed from the initial state to the final state where the RNT is internalized in the vesicle. It is clearly shown that the translocation time is inversely proportional to the rotational frequencies, with high rotational frequencies shortening the translocation time of the nanotube. By data fitting, the translocation time is demonstrated to be logarithmically dependent on the rotational frequencies with the estimated relationship $-558.9 \ln(x) + 2366$. This relationship is in good agreement with the water flux generated by a rotating CNT showing approximately logarithmic dependence on the angular velocity of rotation.[46] At low rotational frequencies, the disturbance caused by the RNT is neutralized by the dynamics of the water particles. However, without the RNT, the vesicle barely changes its position. For better analysis of the fundamental driving force, a rotational torque generated by the RNT can be estimated from the rotational speed of the RNT. Under the simplication of the RNT as a rotating cylinder, the rotational torque (T) is obtained by the equations $T = \gamma\omega$, $\gamma = [(1/3)\pi\eta L^3]/[\ln(L/2r) - 0.66]$, where γ is the rotational drag coefficient, ω is the rotational speed, η is the viscosity of the environmental solution, L is the length of the cylinder, and r is the radius of the cylinder.[47] Here we take $\eta = 1$ mPa·s (pure water), $L = 10r_c$,

DOI: 10.1021/acs.jpclett.5b00755
J. Phys. Chem. Lett. 2015, 6, 2530−2537

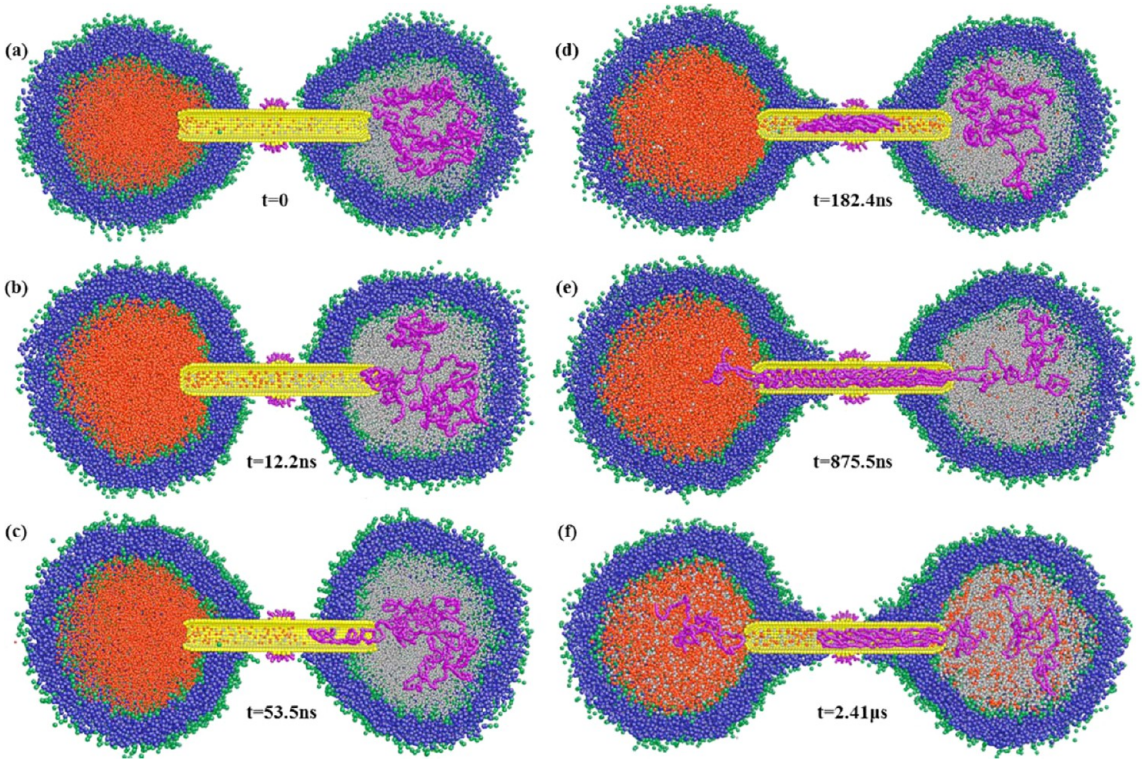

Figure 7. Evolution of polymer chain transportation between two vesicles through the RNT channel. Water beads in vesicle A are shown in brown, while water beads from vesicle B are shown in white.

and $r = 2.0r_c$. As a result, the rotational torque is calculated to be in the range of 0.54−0.0056 nN·m. Therefore, by tailoring the rotational frequeny of the RNT, we can manipulate the rotational torque of the RNT in a range of $\sim 10^{-1}$ to $\sim 10^{-3}$ nN·m to control the internalization process of the nanotube. More interestingly, the internalized RNT with a hollow cavity can be embedded into the lipid membrane, acting like a bological ionic channel,[13] which will offer useful insights into designing RNT-based devices for exchanging substances with cells.

RNT−Vesicle Network. Due to the extremely small size, high surface energy, and high surface area of the NP, the interaction between cells and NPs can be heavily influenced by intelligent surface structure designs.[48−51] The ligand coating on the NP is a general way to manipulate the NP properties. For example, cellular uptake of NPs coated with various ligands is known to be strongly influenced by the polymer pattern on the NP surface.[50,52−54] In the experiment, dopamine was demonstrated as a robust molecular anchor to link functional molecules such as nitrilotriacetic acid to the shell of magnetic NPs, which possessed high stability and specificity for separating histidine-tagged proteins.[55] Similarly, RNTs with a properly functionalized surface will be equipped with enhanced functionality that allows them to selectively attach to target cells or tissues and play a therapeutic role. On the basis of the phenomenon observed in Figure 2, a surface-modified RNT is created via an intended rule to avoid the full internalization by the vesicle. The hydrophilic ligands (one hydrophobic head and four hydrophilic tails) are coated on the surface of the middle portion of the RNT. Intuitively, the pure hydrophobic nanotube can enter inside of the vesicle membrane, while the portion of the RNT coated with hydrophilic ligand cannot get through the vesicle membrane when the driving force generated from the rotation is insufficient to overcome the repulsive force due to hydrophobicity of the middle layer. The penetration force for the nanotube coating with the 10 tail hydrophilic ligands is $\sim 190k_BT/r_c$, while the penetration force for a pure hydrophobic nanotube to enter inside of the membrane is $\sim 20k_BT/r_c$.[50] Two ends of the RNT are designed as spherical caps, which introduces minimum disruption on the vesicle membrane during the rotational process.[56] Each cap contains a lipid-size pore to make sure that no membrane lipid can pass it into the RNT. As a comparison, we have performed a simulation and demonstrated that the RNT without a cap presents a similar penetration process into vesicles, but it also breaks the integrity of the vesicle by cutting a portion of membrane into the tube. As expected, the nanotube without a cap causes the disorder of the membrane with a portion of lipid molecules left inside of the tube cavity, which leads to the blockage of the substance exchange process between the vesicles through the channel. The RNT rotates at a fixed rotational frequency of $1/(600\tau)$, and the rotational axis is fixed as well. As shown in Figure 3, two identically sized vesicles are put $5r_c$ away from the tips of the RNT along the rotational axis. As the simulation starts, thanks to the water turbulence generated by the RNT, the two vesicles slowly approach toward the RNT tips followed by the penetration of the hydrophobic tips of RNT into the vesicle membrane. Once the RNT starts to contact with the vesicle, the vesicle quickly internalizes the RNT due to the identical hydrophobicity of the RNT and the vesicle inner layer. It can be clearly observed that a small portion of lipid tails from the membrane climbs up the surface of the RNT during the penetration process. Finally, the two vesicles are adjoined by the RNT, and the system is stabilized to form an artificial channel between them, through which they are capable of exchanging materials and information.

DOI: 10.1021/acs.jpclett.5b00755
J. Phys. Chem. Lett. 2015, 6, 2530−2537

Considerable effort has been devoted to determining the regulatory networks that control and mediate complex biological processes.[57,58] Following the phenomenon captured by interaction between a single RNT and two vesicles, a multicomplex cellular network composed of RNTs and vesicles can be designed if the rotational axes are well controlled. With the same rotational frequency used in Figure 3, we put three RNTs in a triangle shape with three vesicles and fix the rotational axis along the triangle edges, as shown in Figure 4b. The distance between the RNT tips and vesicles is set to be $5r_c$. The rotation direction follows the right-hand rule. Following the similar penetration principle, as the vesicle approaches RNTs, two tips of two RNTs can penetrate the membrane and create a three-RNT−three-vesicle complex network. Similarly, as shown in Figure 4c, four RNTs on the square shape with four vesicles create a four-RNT−four-vesicle complex network. Actually, the *N*-RNT−*N*-vesicle network could be designed by tuning the number and orientation of RNTs and the number and size of vesicles, for example, the four-RNT−one-vesicle network unit shown in Figure 1. However, we should pay attention to the fact that while more RNTs penetrate through the fixed sized vesicle, as shown in Figure 4b′ and c′, the spherical shape of each vesicle would be heavily affected by the unbalanced number of lipids in the inner layer and outer layer of the vesicle membrane from the penetration. The simple composite structure gathered through the analysis of interaction between RNTs and vesicles as a building unit can be assembled into a more complex vesicular network whose topological structure would perform significant and sophisticated biological activities.

Materials Exchange through the RNT Channel. As discussed in the previous section, gap junctions and membrane tubes are both specialized intercellular connection channels and connect the cytoplasm of cells, which allows various molecules, ions, and electrical impulses to directly pass through a regulated gate between cells.[8,59,60] In addition to the molecular weight and size, the ability of a solute to transverse the channel depends on its net charge, shape, and interactions with the specific components the constitute the channel.[61,62] Rules that dictate the ability of a molecule to travel through the channel are complex. Therefore, it is vital to understand how one uses the channel to transport molecules between cells. Especially, insights into the artificial channel between cells are pivotal to control and not just to understand the transport process. From the interaction profile between a single RNT and the two vesicles shown in Figure 3, RNTs with hollow structure can act as potential synthetic channels to mimic intercellular communication. Two different sizes of molecules are employed to demonstrate the transport capability of the RNT-based artificial channel between vesicles. For small particle exchange, we trace the water particles from two vesicles with distinct brown and white color to evidence the exchange. After the RNT forms a stable channel between two vesicles, as shown in Figure 3f, a dynamic evolution of the specialized water particles between two vesicles is depicted in Figure 5. It can be clearly observed that the water beads from two vesicles can slowly diffuse through the RNT channel and enter into each other. The diffusive rate can be described by the term $r = \partial N/\partial t$ in the single direction along the RNT channel, where N is the number of water beads appearing inside one vesicle from the other and t is the time needed to diffuse. The diffusive rate from vesicle A to vesicle B (1.25 beads/ns) is approximately equal to that from vesicle B to vesicle A (1.21 beads/ns). It turns out that the vesicle size plays an important role in the transmission of water through the channel. A different vesicle possesses a different curvature energy, which can influence the internalization of the nanotube and the water exchange between two vesicles. To make a comparison, we study three different sets of two-vesicle−one-RNT systems, as shown in Table 1. It can be noticed that for pattern I, the vesicles with the same size (radius = $12r_c$) possess water diffusion rates of 1.25 beads/ns from vesicle A to vesicle B and 1.21 beads/ns from B to A. With respect to pattern II (the vesicles with the same radius $7r_c$), the diffusion rates of water particles through the channel are 1.27 beads/ns from vesicle A to vesicle B and 1.24 beads/ns from B to A. These two patterns show a very close water diffusion rate. In contrast, when the two vesicles connected by a nanochannel have a different radius such as vesicle A with $12r_c$ and vesicle B with $7r_c$, the diffusion rates of the water particles via the channel are 1.35 beads/ns from vesicle A to vesicle B and 1.32 beads/ns from B to A. The noticeable discrepancy of the water diffusion rate in the heterosystem (pattern II) from the homosystems (patterns I and III) may be attributed to the pressure imbalance caused by the curvature energy difference inside of the systems. It is obvious that the curvature energy difference of the heterosystem is larger than that in the homosystem. Here, the rotation is turned off after RNT protrudes into the vesicle, therefore eliminating the effect of the nanotube rotation on the order of the vesicle membrane.[19] To make comparison while the rotation is turned on for pattern I, the diffusion rate of water particles is estimated as 1.36 beads/ns from vesicle A to vesicle B and 1.32 beads/ns from vesicle B to vesicle A, with a slight difference from the results without the rotation.

Similar to the one-RNT−two-vesicle network, the model from Figure 4a is applied to investigate the transporting function of RNT channels on the three-RNT−three-vesicle network in Figure 6. The number of water beads coming from two other vesicles bridged by the RNT channel is documented to present the efficiency of the transport by channels. The diffusive rate from vesicle B and vesicle C to vesicle A is estimated to be 0.62 beads/ns, which is close to the water beads flow to the other two vesicles. The reason for the low diffusive rate compared to Figure 5 can be attributed to the morphology change of vesicles as well as the low possibility for outbound water beads from the more open RNT channel. As two tips of RNTs penetrate the vesicle, they instigate a change in the morphologies of the spherical vesicles to more crescent-like shapes, as shown in Figures 4 and 6. The diffusion rate slightly decreases when the concentration of exotic water beads from mutual vesicles reachs the equilibrium state. More precisely, the overall slope of the curves in Figure 6 is in good agreement with the observation in Figure 5.

Different from the water bead transport, the exchange of genetic information in bacteria and many viruses encoded in DNA macromolecules is critical to the proliferation and replication of cells. The transfer of genetic information is one of several ways to replicate the genome for inheritance of genetically determined traits. By creating a bridge-like connection between two cells, the conjugation will transfer genetic material from the donor to the recipient, which can include such genetic information as antibiotic resistance or the ability to use new metabolites.[63] To mimic this kind of transfer activity and further demonstrate the benefits of gap channel regulating properties, we simulate the transportation of a long polymer chain (considered to be a DNA chain) from one vesicle to another through a connecting RNT channel. As

DOI: 10.1021/acs.jpclett.5b00755
J. Phys. Chem. Lett. 2015, 6, 2530−2537

shown in Figure 7, three polymer chains composed of 360 hydrophilic beads each are initially put inside of one vesicle when the RNT channel bridges two vesicles, as seen in Figure 7a. The polymer beads have the same properties as the hydrophilic ligand beads, and consecutive beads are connected with bonds (k_S = 200.0, r_S = 0.25). It can be noticed that the head of one chain starts to diffuse into the RNT tip and then fully enters inside of the RNT channel, as shown in Figure 7b. Following the first chain, the second chain also enters inside of the RNT channel. Due to the hydrophilicity inside of the vesicle on the left shown in Figure 7c, a portion of the chain enters into another vesicle and diffuses out of the RNT channel. On the contrary, the second chain is caught when it enters inside of the RNT channel due to its coiled tail. The transport of a whole polymer chain through the RNT channel is dominated by the autonomous self-diffusion process without any other driving mechanism. These intriguing and motivating simulation results lend credence to show that the RNT channel can act as a promising synthetic channel to regulate the exchange of substances between vesicles such as water molecules and DNA-like chain. Also, our study can offer useful insight into designing biomedical nanodevices for complex biological intercellular activities.

In summary, we have performed dissipative dynamics simulation in order to investigate how RNTs affect their local environment and trigger the movement of adjacent vesicles by controlling the rotational axis. The translocation time needed for the RNT to protrude into the vesicle decreases with the increase of the rotational frequency. Our simulation suggests that a RNT with a patterned surface can create an intercellular channel between vesicles to form a complex vesicular network that facilitates the vesicle-to-vesicle communication. The RNT channel does not structurally deteriorate the integrity of the vesicle while it keeps the exchange of small molecules and macromolecules between vesicles. There is also plenty of room for further exploration on modifying the RNT shape and charge to dramatically alter its selectivity, opening up possibilities for its use in biological fields. For example, cell swelling generally occurs because of the osmotic pressure created either by an ionic imbalance or by a lack of nutrients. Either way, the cell expands to cope with the imbalance of the chemicals that it needs through the RNT channel to maintain its metabolism. To accelerate the diffusion, a hydrostatic pressure difference between the two vesicles can be established to produce a net directional water flow from one vesicle to another vesicle.[64] Our fundamental simulation findings provide promising guidance for designing a novel synthetic channel for cell-to-cell communication.

AUTHOR INFORMATION

Corresponding Author

*E-mail: xqwang@uga.edu. Tel: 706-542-6251.

Notes

The authors declare no competing financial interest.

ACKNOWLEDGMENTS

The authors acknowledge the support from the University of Georgia (UGA) start-up fund. The facility support for modeling and simulations from the UGA Advanced Computing Resource Center is greatly appreciated.

REFERENCES

(1) Bassler, B. L. Small Talk: Cell-to-Cell Communication in Bacteria. *Cell* **2002**, *109*, 421−424.
(2) Loewenstein, W. R. Junctional Intercellular Communication: the Cell-to-Cell Membrane Channel. *Physiol. Rev.* **1981**, *61*, 829−913.
(3) Waters, C. M.; Bassler, B. L. Quorum Sensing: Cell-to-Cell Communication in Bacteria. *Annu. Rev. Cell Dev. Biol.* **2005**, *21*, 319−346.
(4) Ezzell, C. Cell-to-Cell Communication. *Nature* **1989**, *337*, 388−392.
(5) Kumar, N. M.; Gilula, N. B. The Gap Junction Communication Channel. *Cell* **1996**, *84*, 381−388.
(6) Goldberg, G. S.; Valiunas, V.; Brink, P. R. Selective Permeability of Gap Junction Channels. *Biochim. Biophys. Acta, Biomembr.* **2004**, *1662*, 96−101.
(7) Nakano, T.; Suda, T.; Koujin, T.; Tokuko, H.; Hiraoka, Y. Bio-Inspired Models of Network, Information and Computing Systems. *Molecular Communication through Gap Junction Channels: System Design, Experiments and Modeling*, 2nd ed.; Bionetics: Yorktown, VA, 2007; pp 139−146.
(8) Zhang, J.; Zhang, Y. Membrane Nanotubes: Novel Communication between Distant Cells. *Sci. China Life Sci.* **2013**, *56*, 994−999.
(9) Tarakanov, A. O.; Goncharova, L. B. Cell−Cell Nanotubes. *Commun. Integr. Biol.* **2009**, *2*, 359−361.
(10) Sherer, N. M. Long-Distance Relationships: Do Membrane Nanotubes Regulate Cell−Cell Communication and Disease Progression? *Mol. Biol. Cell* **2013**, *24*, 1095−1098.
(11) Sowinski, S.; Jolly, C.; Berninghausen, O.; Purbhoo, M. A.; Chauveau, A.; Kohler, K.; Oddos, S.; Eissmann, P.; Brodsky, F. M.; Hopkins, C.; Onfelt, B.; Sattentau, Q.; Davis, D. M. Membrane Nanotubes Physically Connect T Cells over Long Distances Presenting a Novel Route for HIV-1 Transmission. *Nat. Cell Biol.* **2008**, *10*, 211−219.
(12) Chauveau, A.; Aucher, A.; Eissmann, P.; Vivier, E.; Davis, D. M. Membrane Nanotubes Facilitate Long-Distance Interactions between Natural Killer Cells and Target Cells. *Proc. Natl. Acad. Sci. U.S.A.* **2010**, *107*, 5545−5550.
(13) Geng, J.; Kim, K.; Zhang, J.; Escalada, A.; Tunuguntla, R.; Comolli, L. R.; Allen, F. I.; Shnyrova, A. V.; Cho, K. R.; Munoz, D.; Wang, Y. M.; Grigoropoulos, C. P.; Ajo-Franklin, C. M.; Frolov, V. A.; Noy, A. Stochastic Transport through Carbon Nanotubes in Lipid Bilayers and Live Cell Membranes. *Nature* **2014**, *514*, 612−615.
(14) Franceschini, L.; Soskine, M.; Biesemans, A.; Maglia, G. A Nanopore Machine Promotes the Vectorial Transport of DNA across Membranes. *Nat. Commun.* **2013**, *4*, 2415.
(15) Sholl, D. S.; Johnson, J. K. Making High-Flux Membranes with Carbon Nanotubes. *Science* **2006**, *312*, 1003−1004.
(16) Langecker, M. Synthetic Lipid Membrane Channels Formed by Designed DNA Nanostructures. *Science* **2012**, *338*, 932−936.
(17) Seifert, A.; Göpfrich, K.; Burns, J. R.; Fertig, N.; Keyser, U. F.; Howorka, S. Bilayer-Spanning DNA Nanopores with Voltage-Switching between Open and Closed State. *ACS Nano* **2015**, *9*, 1117−1126.
(18) Dutt, M.; Kuksenok, O.; Little, S. R.; Balazs, A. C. Forming Transmembrane Channels Using End-Functionalized Nanotubes. *Nanoscale* **2011**, *3*, 240−250.
(19) Yue, T.; Zhang, X.; Huang, F. Molecular Modeling of Membrane Responses to the Adsorption of Rotating Nanoparticles: Promoted Cell Uptake and Mechanical Membrane Rupture. *Soft Matter* **2015**, *11*, 456−465.
(20) Li, Y.; Li, X.; Li, Z.; Gao, H. Surface-Structure-Regulated Penetration of Nanoparticles Across a Cell Membrane. *Nanoscale* **2012**, *4*, 3768−3775.
(21) Li, Y.; Yuan, H.; von dem Bussche, A.; Creighton, M.; Hurt, R. H.; Kane, A. B.; Gao, H. Graphene Microsheets Enter Cells through Spontaneous Membrane Penetration at Edge Asperities and Corner Sites. *Proc. Natl. Acad. Sci. U.S.A.* **2013**, *110*, 12295−12300.
(22) Zhao, Z.; Huang, D.; Yin, Z.; Chi, X.; Wang, X.; Gao, J. Magnetite Nanoparticles as Smart Carriers to Manipulate the

DOI: 10.1021/acs.jpclett.5b00755
J. Phys. Chem. Lett. 2015, 6, 2530−2537

Cytotoxicity of Anticancer Drugs: Magnetic Control and Ph-Responsive Release. *J. Mater. Chem.* **2012**, *22*, 15717−15725.
(23) Mody, V.; Cox, A.; Shah, S.; Singh, A.; Bevins, W.; Parihar, H. Magnetic Nanoparticle Drug Delivery Systems for Targeting Tumor. *Appl. Nanosci.* **2014**, *4*, 385−392.
(24) Zhang, E.; Kircher, M. F.; Koch, M.; Eliasson, L.; Goldberg, S. N.; Renström, E. Dynamic Magnetic Fields Remote-Control Apoptosis via Nanoparticle Rotation. *ACS Nano* **2014**, *8*, 3192−3201.
(25) Liu, D.; Wang, L.; Wang, Z.; Cuschieri, A. Magnetoporation and Magnetolysis of Cancer Cells via Carbon Nanotubes Induced by Rotating Magnetic Fields. *Nano Lett.* **2012**, *12*, 5117−5121.
(26) Wilhelm, C.; Gazeau, F. Magnetic Nanoparticles: Internal Probes and Heaters Within Living Cells. *J. Magn. Magn. Mater.* **2009**, *321*, 671−674.
(27) Bañobre-López, M.; Teijeiro, A.; Rivas, J. Magnetic Nanoparticle-Based Hyperthermia for Cancer Treatment. *Rep. Prac. Oncol. Radiother.* **2013**, *18*, 397−400.
(28) Groot, R. D.; Rabone, K. L. Mesoscopic Simulation of Cell Membrane Damage, Morphology Change and Rupture by Nonionic Surfactants. *Biophys. J.* **2001**, *81*, 725−736.
(29) Groot, R. D.; Warren, P. B. Dissipative Particle Dynamics: Bridging the Gap between Atomistic and Mesoscopic Simulation. *J. Chem. Phys.* **1997**, *107*, 4423−4435.
(30) Li, X.; Liu, Y.; Wang, L.; Deng, M.; Liang, H. Fusion and Fission Pathways of Vesicles from Amphiphilic Triblock Copolymers: A Dissipative Particle Dynamics Simulation Study. *Phys. Chem. Chem. Phys.* **2009**, *11*, 4051−4059.
(31) Shillcock, J. C.; Lipowsky, R. Tension-Induced Fusion of Bilayer Membranes and Vesicles. *Nat. Mater.* **2005**, *4*, 225−228.
(32) Plimpton, S. Fast Parallel Algorithms for Short-Range Molecular Dynamics. *J. Comput. Phys.* **1995**, *117*, 1−19.
(33) Nielsen, S. O.; Ensing, B.; Ortiz, V.; Moore, P. B.; Klein, M. L. Lipid Bilayer Perturbations around a Transmembrane Nanotube: A Coarse Grain Molecular Dynamics Study. *Biophys. J.* **2005**, *88*, 3822−3828.
(34) Venturoli, M.; Smit, B.; Sperotto, M. M. Simulation Studies of Protein-Induced Bilayer Deformations, and Lipid-Induced Protein Tilting, on a Mesoscopic Model for Lipid Bilayers with Embedded Proteins. *Biophys. J.* **2005**, *88*, 1778−1798.
(35) Darnton, N. C.; Turner, L.; Rojevsky, S.; Berg, H. C. On Torque and Tumbling in Swimming Escherichia coli. *J. Bacteriol.* **2007**, *189*, 1756−1764.
(36) DiLuzio, W. R.; Turner, L.; Mayer, M.; Garstecki, P.; Weibel, D. B.; Berg, H. C.; Whitesides, G. M. Escherichia coli Swim on the Right-Hand Side. *Nature* **2005**, *435*, 1271−1274.
(37) Zhang, L.; Abbott, J. J.; Dong, L.; Peyer, K. E.; Kratochvil, B. E.; Zhang, H.; Bergeles, C.; Nelson, B. J. Characterizing the Swimming Properties of Artificial Bacterial Flagella. *Nano Lett.* **2009**, *9*, 3663−3667.
(38) Kumar, V.; Nath, G.; Kotnala, R. K.; Saxena, P. S.; Srivastava, A. Biofunctional Magnetic Nanotube Probe for Recognition and Separation of Specific Bacteria from a Mixed Culture. *RSC Adv.* **2013**, *3*, 14634−14641.
(39) Gao, C.; Li, W.; Morimoto, H.; Nagaoka, Y.; Maekawa, T. Magnetic Carbon Nanotubes: Synthesis by Electrostatic Self-Assembly Approach and Application in Biomanipulations. *J. Phys. Chem. B* **2006**, *110*, 7213−7220.
(40) White, F. M. *Viscous Fluid Flow*, 2 ed.; McGraw-Hill: New York, 1991.
(41) Hangarter, C. M.; Myung, N. V. Magnetic Alignment of Nanowires. *Chem. Mater.* **2005**, *17*, 1320−1324.
(42) Fujiwara, M.; Oki, E.; Hamada, M.; Tanimoto, Y.; Mukouda, I.; Shimomura, Y. Magnetic Orientation and Magnetic Properties of a Single Carbon Nanotube. *J. Phys. Chem. A* **2001**, *105*, 4383−4386.
(43) Jia, X.; Li, W.; Xu, X.; Li, W.; Cai, Q.; Yang, X. Numerical Characterization of Magnetically Aligned Multiwalled Carbon Nanotube−Fe_3O_4 Nanoparticle Complex. *ACS Appl. Mater. Interfaces* **2015**, *7*, 3170−3179.
(44) Kim, K.; Xu, X.; Guo, J.; Fan, D. L. Ultrahigh-Speed Rotating Nanoelectromechanical System Devices Assembled from Nanoscale Building Blocks. *Nat. Commun.* **2014**, *5*, 3632.
(45) Ghosh, A.; Fischer, P. Controlled Propulsion of Artificial Magnetic Nanostructured Propellers. *Nano Lett.* **2009**, *9*, 2243−2245.
(46) Feng, J.-W.; Ding, H.-M.; Ren, C.-L.; Ma, Y.-Q. Pumping of Water by Rotating Chiral Carbon Nanotube. *Nanoscale* **2014**, *6*, 13606−13612.
(47) Howard, J. *Mechanics of Motor Proteins and the Cytoskeleton*; Palgrave Macmillan:London, 2001.
(48) Verma, A.; Uzun, O.; Hu, Y.; Hu, Y.; Han, H.-S.; Watson, N.; Chen, S.; Irvine, D. J.; Stellacci, F. Surface-Structure-Regulated Cell-Membrane Penetration by Monolayer-Protected Nanoparticles. *Nat. Mater.* **2008**, *7*, 588−595.
(49) Nel, A. E.; Madler, L.; Velegol, D.; Xia, T.; Hoek, E. M. V.; Somasundaran, P.; Klaessig, F.; Castranova, V.; Thompson, M. Understanding Biophysicochemical Interactions at the Nano-Bio Interface. *Nat. Mater.* **2009**, *8*, 543−557.
(50) Zhang, L.; Becton, M.; Wang, X. Designing Nanoparticle Translocation through Cell Membranes by Varying Amphiphilic Polymer Coatings. *J. Phys. Chem. B* **2015**, *119*, 3786−3794.
(51) Yang, K.; Ma, Y.-Q. Computer Simulation of the Translocation of Nanoparticles with Different Shapes across a Lipid Bilayer. *Nat. Nanotechnol.* **2010**, *5*, 579−583.
(52) Ding, H. M.; Ma, Y. Q. Role of Physicochemical Properties of Coating Ligands in Receptor-Mediated Endocytosis of Nanoparticles. *Biomaterials* **2012**, *33*, 5798−5802.
(53) Li, Y.; Kröger, M.; Liu, W. K. Endocytosis of Pegylated Nanoparticles Accompanied by Structural and Free Energy Changes of the Grafted Polyethylene Glycol. *Biomaterials* **2014**, *35*, 8467−8478.
(54) Ding, H. M.; Tian, W. D.; Ma, Y. Q. Designing Nanoparticle Translocation through Membranes by Computer Simulations. *ACS Nano* **2012**, *6*, 1230−1238.
(55) Xu, C.; Xu, K.; Gu, H.; Zheng, R.; Liu, H.; Zhang, X.; Guo, Z.; Xu, B. Dopamine as A Robust Anchor to Immobilize Functional Molecules on the Iron Oxide Shell of Magnetic Nanoparticles. *J. Am. Chem. Soc.* **2004**, *126*, 9938−9939.
(56) Shi, X.; von dem Bussche, A.; Hurt, R. H.; Kane, A. B.; Gao, H. Cell Entry of One-Dimensional Nanomaterials Occurs by Tip Recognition and Rotation. *Nat. Nanotechnol.* **2011**, *6*, 714−719.
(57) Barabasi, A.-L.; Oltvai, Z. N. Network Biology: Understanding the Cell's Functional Organization. *Nat. Rev. Genet.* **2004**, *5*, 101−113.
(58) Ma'ayan, A.; Jenkins, S. L.; Neves, S.; Hasseldine, A.; Grace, E.; Dubin-Thaler, B.; Eungdamrong, N. J.; Weng, G.; Ram, P. T.; Rice, J. J.; Kershenbaum, A.; Stolovitzky, G. A.; Blitzer, R. D.; Iyengar, R. Formation of Regulatory Patterns During Signal Propagation in a Mammalian Cellular Network. *Science* **2005**, *309*, 1078−1083.
(59) White, T. W.; Paul, D. L. Genetic Diseases and Gene Knockouts Reveal Diverse Connexin Functions. *Annu. Rev. Physiol.* **1999**, *61*, 283−310.
(60) Maeda, S.; Nakagawa, S.; Suga, M.; Yamashita, E.; Oshima, A.; Fujiyoshi, Y.; Tsukihara, T. Structure of the Connexin 26 Gap Junction Channel at 3.5Å Resolution. *Nature* **2009**, *458*, 597−602.
(61) Majumder, M.; Chopra, N.; Hinds, B. J. Mass Transport through Carbon Nanotube Membranes in Three Different Regimes: Ionic Diffusion and Gas and Liquid Flow. *ACS Nano* **2011**, *5*, 3867−3877.
(62) Liu, X.; Pan, X.; Zhang, S.; Han, X.; Bao, X. Diffusion of Water Inside Carbon Nanotubes Studied by Pulsed Field Gradient NMR Spectroscopy. *Langmuir* **2014**, *30*, 8036−8045.
(63) Holmes, R. K.; Jobling, M. G. Genetics. In Baron, S., Ed.; *Medical Microbiology*, 4th ed.; University of Texas Medical Branch: Galveston, TX, 1996; Chapter 5.
(64) Zhu, F.; Tajkhorshid, E.; Schulten, K. Pressure-Induced Water Transport in Membrane Channels Studied by Molecular Dynamics. *Biophys. J.* **2002**, *83*, 154−160.

DOI: 10.1021/acs.jpclett.5b00755
J. Phys. Chem. Lett. 2015, 6, 2530−2537